Chapter 2

Background

AN understanding of the continuous casting process is necessary so that the methods used in later chapters can be fully comprehended. This chapter aims to inform the reader of the literature regarding the subject matter and the techniques that are used in this thesis.

A brief description of the continuous casting process which highlights the main functional units is given in §2.1. In §2.2.1, a review is given of the literature regarding the causes or influencing factors of defects in the process. The review is rather detailed, because a thorough understanding of the defects and their causes gives greater insight into the design of a defect predictor. This section also describes several models for defect propagation and prediction found in literature.

§2.2.2 describes specific statistical hypothesis tests that are used in chapter 3. These hypothesis tests are known as goodness-of-fit tests and determine whether data come from a given theoretical distribution. The hypothesis tests will be used to reduce the number of variables that are present for a defect prediction model.

Correlation analysis is described in §2.2.3. The correlation can be used to detect one-to-one relationships of variables so that the number of variables can be reduced in a prediction model. If one-to-one relationships do exist, the model size is reduced to avoid repetition of information.

The Box-Jenkins [31] type modelling strategy known as ARX (Auto Regression with eXogenous input) is described in §2.2.4. This form of system identification is popular for the determination of empirical linear system models used for control system design. The tech-

nique will be applied to the current control / modelling problem. A brief overview of the system identification technique will be given.

A controller for a SIMO type system that can track set-points will be described in §2.2.5. The controller forms part of an optimal set of controllers based on the solution of the Riccati equation. The controller is designed for steady-state operation. The design of this controller is simple, and guarantees system stability. The design procedure will be covered briefly. This controller is one of three controllers that will be compared to improve the response of the system. The other controllers are simple to understand and will not be explained in this chapter.

2.1 Continuous casting process

The description of the continuous casting process is done for a *bow-type* continuous caster (see Fig. 2.1) since it is the most predominant caster found in practice. Each critical component of the caster is described [1].

2.1.1 Ladle

Molten steel arrives at the continuous casting machine in a container known as the ladle. In steel casters, the ladle contains between 70-300 tons of molten steel at between 1500 and 1600 °C [1]. The ladle is then placed on one end of a rotating platform known as the turntable. The turntable can accommodate at least two ladles simultaneously. When all the steel from one ladle is cast, the turntable swings around and casting proceeds from the second ladle. This method of ladle switching ensures that steel is usually available for casting. The turntable method is the most widely used mechanism to switch ladles. Some casters use a slide mechanism by which the ladle is slid into position before casting commences. However, this method causes a long delay between switching because one ladle has to be extracted before another ladle can be slid into position. At the bottom of the ladle there is usually a slide-gate mechanism that controls the rate of flow of molten steel into another container known as the tundish.

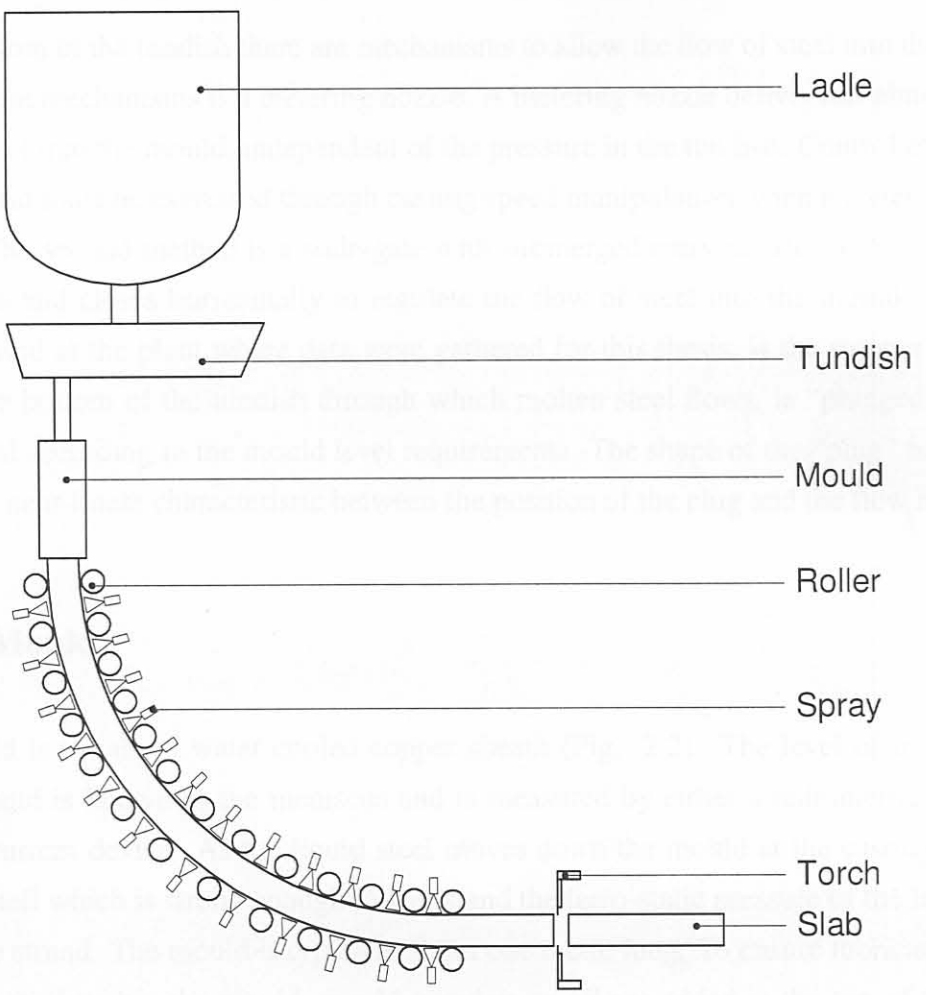

Figure 2.1 Side view of a bow-type continuous caster

2.1.2 Tundish

The tundish acts as a reservoir of molten steel. The reason that liquid metal is not poured directly into the mould from the ladle is three-fold. Firstly, if a ladle is not available for casting, continuity is not assured. Secondly, the tundish is designed to accommodate complex mechanisms to control the flow of steel into the mould. Thirdly, the tundish can be designed to provide liquid steel to several moulds as is the case with multi-strand casters.

At the bottom of the tundish there are mechanisms to allow the flow of steel into the mould[a]. One of these mechanisms is a metering nozzle. A metering nozzle delivers an almost steady flow of steel into the mould, independent of the pressure in the tundish. Control of the level in the mould must be exercised through casting speed manipulation when a metering nozzle is used. The second method is a slide-gate with submerged entry nozzle (SEN). The slide-gate opens and closes horizontally to regulate the flow of steel into the mould. The third method, used at the plant where data were gathered for this thesis, is the stopper rod. The hole at the bottom of the tundish through which molten steel flows, is "plugged up" by a stopper rod according to the mould level requirements. The shape of the "plug" is designed to allow a near-linear characteristic between the position of the plug and the flow rate.

2.1.3 Mould

The mould is usually a water cooled copper sheath (Fig. 2.2). The level of molten steel in the mould is known as the meniscus and is measured by either a radiometric device or an eddy current device. As the liquid steel moves down the mould at the casting speed, it forms a shell which is strong enough to withstand the ferro-static pressure of the liquid steel within the strand. The mould is typically about one metre long. To ensure lubrication of the solidified shell within the mould, mould powders or oil are added at the top of the mould [33]. These additives form a thin crystalline layer as well as a liquid layer between the steel and the copper plate (sheath) to reduce friction. The fluxes also provide insulation from the atmosphere at the top of the mould to prevent oxidation. Sometimes the mould flux is insufficiently distributed along the mould, or the mould is too hot so that the strand surface fuses with the mould surface. This is known as a sticker break-out and results in tearing of the strand shell so that liquid steel pours out from beneath the mould. Break-outs are extremely costly because of losses due to scrapping of steel and destruction of equipment by the liquid metal which results in down-time. Special thermocouples are sometimes inserted

[a] see *e.g.* Hill and Wilson [32] for a discussion on the importance of the design of the mould inflow

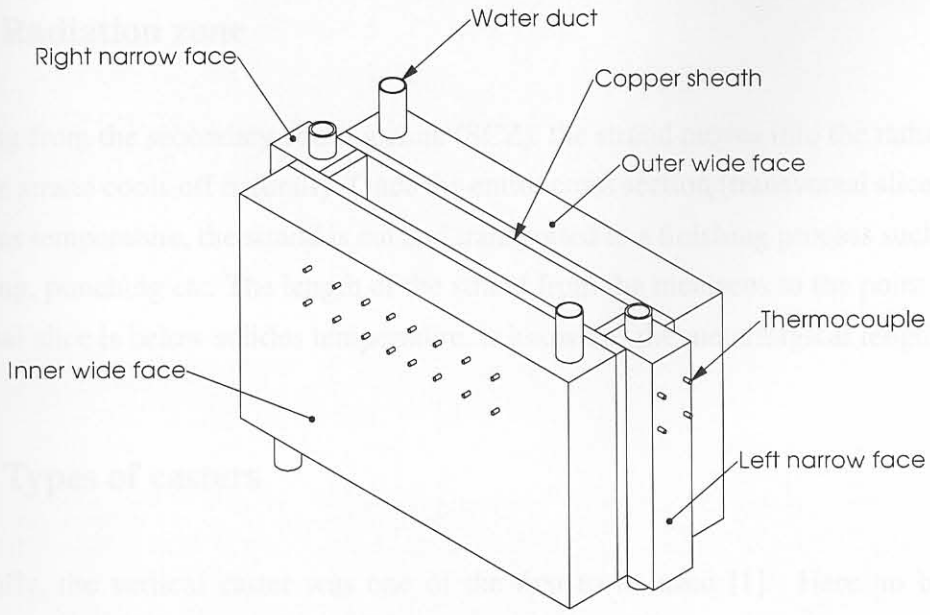

Figure 2.2 Isometric view of a continuous caster mould.

in the mould to measure temperature gradients from the top to the bottom of the mould. Should the temperature gradient be too large, a break-out may occur. The thermocouples act as a break-out-detector, warning the operator of possible break-outs. The mould oscillates to aid in the extraction of the solidified strand (see *e.g.* Burgess, Guzman, and Singh [34]). The mould width is adjustable by moving the narrow sides in or out. Typical widths for slab casters are 1000mm, 1280mm and 1575mm.

2.1.4 Secondary cooling zone

On exit from the mould, the strand enters the secondary cooling zone which ranges in length from 6 to 20 metres. Directly below the mould there is usually a device known as the spray ring which provides water flow to the strand to aid in cooling, and to ensure a smooth heat-transfer gradient between the mould and secondary cooling zone. In the secondary cooling zone, rollers support the strand and aid in bending and straightening in the case of bow type casters. Water sprays extract the heat from the strand. These sprays are grouped in three to six spray zones. Water flow in each spray zone is independently controlled by valves.

2.1.5 Radiation zone

On exiting from the secondary cooling zone (SCZ), the strand moves into the radiation zone where the strand cools off naturally. Once the entire cross section (transversal slice) is below the solidus temperature, the strand is cut and transported to a finishing process such as grinding, rolling, punching *etc.* The length of the strand from the meniscus to the point where the transversal slice is below solidus temperature, is known as the metallurgical length.

2.1.6 Types of casters

Historically, the vertical caster was one of the first to be used [1]. Here no bending or straightening is required but the machine needs considerable physical space and there are serious shape problems due to gravity adversely affecting the flow of steel. The bow caster was the next in the casting evolution and is the most widely used casting method today. One of the newest types of casters is the horizontal continuous casting process whereby casting is performed horizontally. The only real disadvantage of bow casting compared to the other two mentioned is that the bow caster requires the bending and subsequent straightening of the strand which might lead to some surface imperfections.

2.1.7 New caster technologies

The major parameter by which the success of any casting process is measured, is its throughput over all unit processes. The throughput is the amount of steel cast as a function of time. A thinner strand cools down quicker, but less steel is cast. This trade-off actually swings totally towards faster cooling times because the relationship between cooling time (t) and section thickness (l) is not linear ($t \propto l^2$) [35]. Since the strand is now thinner, rolling throughput is increased.

Current development in continuous casting includes thin-slab casting and strip casting (see *e.g.* Brückner [36]). Thin-slab casting is a fairly established technology and this type of caster has found its place in many steel companies. Strip casting is a method by which rollers are used to cool the molten metal while simultaneously forcing a thin shape; and is currently being implemented at some steel-making companies.

2.2 Literature overview

This section describes the most relevant literature which was found regarding the scope of this thesis.

2.2.1 Defects

There are several defects that occur when continuous casting is applied. Any defects in a solidifying strand are primarily caused by the mould [37]. The secondary cooling zone can only compound the defect, not eradicate it.

The primary control problem in continuous casting is the level of steel in the mould. The level of steel in the mould should not vary much, but remain as constant as possible. The *mould level control problem* is the main problem that is addressed by control system researchers in the field of continuous casting[b]. Mould level oscillations tend to cause depressed regions filled with solidified mould powders, resulting in surface defects. Until now, researchers have not been able to agree on the causes of mould level oscillation though many theories exist [49].

Some of the metallurgical and mechanical problems that arise in continuous casting are summarized by Brimacombe and Samarasekera [50, pp. 182–185]:

1. The *cleanliness* of the steel can be affected *e.g.* there can be
   - oxidation of steel with oxygen from air or refractories,
   - pickup of exogenous inclusions [51, 52] from ladle and tundish refractories and mould powders,
   - bad control of fluid flow in the tundish so that inclusions do not float out,
   - bad mould powder and startup/shutdown procedures, causing break-outs.
2. *Cracks* occurring in, or on the steel such as [53, 54]

[b] see *e.g.* De Keyser [38], De Keyser [39], Inkinen, Lautala, and Saarelainen [40], Kong and De Keyser [41], Graebe, Goodwin, and Elsley [42], Jenkins, Thomas, Chen, and Mahapatra [43], Nilles and Marique [44], Mellberg [45], Hesketh, Clements, and Williams [46], Hattori, Nagata, Inaba, Ishitobi, Yamamoto, Okada, and Zeze [47] and Andrzejewski, Köhler, and Pluschkell [48]

- surface cracks which are a serious quality problem because the cracks oxidize and give rise to oxide-rich seams in the rolled product or, to an even greater extent, cause the strand to be scrapped due to extremely deep longitudinal cracks [55], and
- internal cracks which can also be a problem particularly if during rolling, they do not close, leaving voids in the steel product.
- As the strand moves from one cooling zone to the next, changes in heat extraction cause 1) shifts in thermal gradients through the solidifying shell and 2) stress generation resulting from differential expansion or contraction [56, 57].

3. *Macro-segregation.* There are higher concentrations of certain elements in certain regions of the strand, causing cracks during rolling [58].
4. Cross sectional or *transverse shape.* Deviations from the specified shape due to non-homogeneous cooling in the mould requires excessive reworking.

Though many types of defects occur in continuous casting, the defects discussed here are limited to those specified by personnel at the steel-making plant as well as the available data. The first limitation is that only surface defects are considered. Internal defects fall outside the scope of this thesis; and, after all, the surface defects are the reason for the grinding process. Secondly, only variables present in the mould are used as the parameters under investigation. This means that defects which arise in *e.g.* the secondary cooling zone are not considered. Because of the aforementioned limitation, the compounding effect which the secondary cooling zone has on some defects that start in the mould could possibly not show in the mould variables. The same type of reasoning can be followed for the tundish; except that the tundish precedes the mould in the process and therefore *does* have an influence on mould variables (*e.g.* mould level). Therefore, one can assume that a surface defect that occurs due to some varying parameter in the tundish should be visible in the mould parameters.

The defects which do occur during casting operation at the industrial partner are discussed in the following sections, with specific emphases on their descriptions and causes.

2.2.1.1 Transversal cracking (defect 1a)

The occurrence of transverse cracks seems to be a problem which occurs frequently around the world, considering the amount of literature found on the subject. Transverse cracking in

general occurs due to fast or uneven cooling, sticking in the mould, and bending or straightening at low temperatures [59][c]. Transversal cracks fall under the general heading of *cracks* as described above (point 2, §2.2.1).

The occurrence of this defect coincides with the occurrence of oscillation marks[d] (§2.2.1.6) and transversal depressions (§2.2.1.8) [69]. The defect is generally not easily noticeable until after the slab has been "dressed" or rolled to plate [70].

The occurrence of transversal cracks is subdivided into transversal corner cracking and transversal facial cracking. These two occurring cracks are discussed in the next sections.

Transversal corner cracks These cracks occur on the radiused or chamfered part of the section, normal to the axis of the product [59]. Fig. 2.3 shows the occurrence of a transversal corner crack in the case of a 9 inch bloom. Transversal corner cracks occur for the following

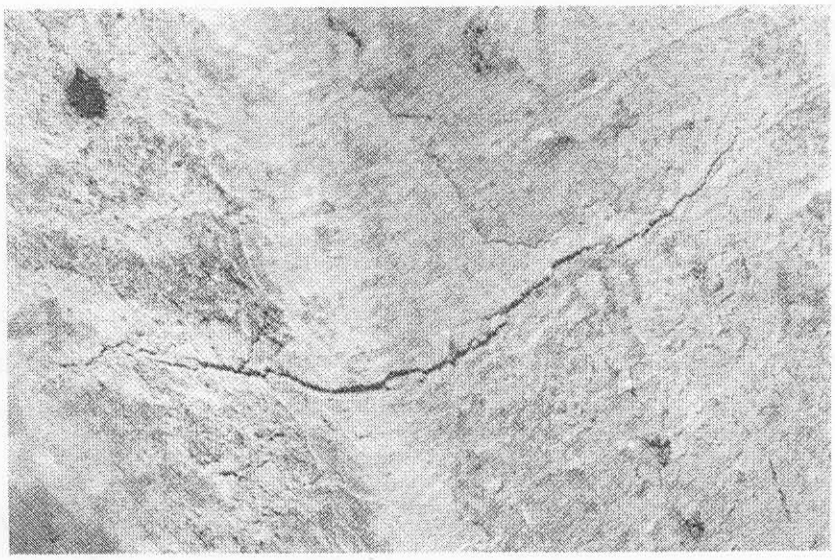

Newton *et al.* [59, p. 5]

Figure 2.3 Transversal corner crack.

reasons.

1. Bending or straightening at temperatures that are too low [59].

[c]see also Mintz, Yue, and Jones [60], Billany, Normanton, Mills, and Grieveson [61], Yasumoto, Maehara, Nagamichi, and Tomono [62], Diener, Drastik, Redenz, and Wagner [63] and Harste and Tacke [64]

[d]see Mintz *et al.* [60], Szekeres [65], Takeuchi and Brimacombe [66], Wolf [67] and Muller [68]

2. Sticking of the product in the mould due to increases in friction of the mould-strand interface [59]. Friction increases occur for several reasons as described by Emling [71], *e.g.* unsuitable mould taper, oscillation, powder and temperature; and casting speed variations.

Composition can be a factor which increases the occurrence of the defect *e.g.* manganese levels higher than 1% with 0.03% vanadium has been found to increase the occurrence of the defect [70] for carbon steels. Brimacombe and Sorimachi [53] further state that aluminium or niobium together with more than 1% manganese increases the chances of occurrence of the defect in carbon steels[e].

The effect generally originates in the mould, but can also originate just below the mould during tension on the strand in a region of low ductility as described by Brimacombe and Sorimachi [53] as well as Saito, Kimura, Ueta, Kimura, Takemoto, and Mine [76].

Uneven water temperature or flow or improper use of mould powders or uneven cooling in the mould which leads to rhomboicity in billets and blooms can also form longitudinal corner cracks [69].

Transversal facial cracks These cracks are defined by Newton *et al.* [59, p. 6] as "a crack not on the radiused or chamfered part of the section, normal to the axis of the product". A drawing of the defect is given in Fig. 2.4. The main causes that are associated with this crack is given below [59].

1. Too severe cooling in the mould or sprays (in the case of large sections such as slabs).
2. Sticking in the mould due to friction.

Leclerc and Pollak [77] state that transversal depressions originate in the mould and may occur due to the oscillation cycle and the entrapment of mould powder at the corner of the slab. The cracks occur at the bottom of the oscillation marks [53, 76, 77] due to a frictional irregularity which is caused by the weakening effect of entrapped mould powder below the oscillation mark upon flattening. To eradicate this problem, the negative strip ratio[f] should

[e] See the articles by Mintz [72], Burden, Funnell, Whitaker, and Young [73], Unger, Biesterfeld, Berentzen, and Thielmann [74] and Razumov, Zabil'skii, Umanets, Lebedev, and Obukhov [75], where reference is made to the detailed influence of N, V, Ti, Cu, Sn, S and P on hot ductility and the occurrence of transversal cracks.

[f] Ratio based on the difference between the average downward velocity of the mould during one oscillation cycle and the casting speed when the mould velocity exceeds the casting speed [65].

not exceed 0.7, and the corners of the mould must not get too cold [77].

Discussion The information on the above mentioned cracks is not sufficient to make a distinction between the two subgroups of cracks (*i.e.* corner and facial cracks), especially since the causes are so similar.

Based on the literature, the mould can cause transversal cracking on the slab surface if the following should happen.

1. Severe cooling in the mould.
2. High friction in the mould.
3. Improper oscillation technique.
4. Carbon steel compositions where 1% manganese is involved.

The mould parameters which would be expected to show the effect of the above mentioned abnormalities are

1. Thermocouple temperatures and longitudinal/transversal temperature gradients, average heat flux, water inlet temperature and flow.

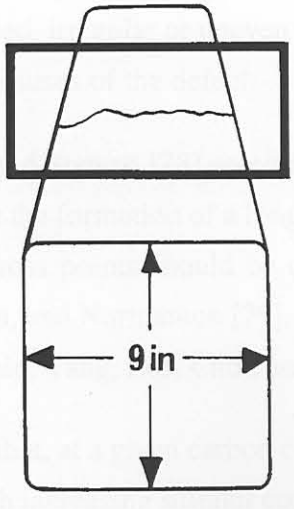

Newton *et al.* [59, p. 6]

Figure 2.4 Transversal facial crack on a 9 inch bloom.

2. Mould powder addition method and composition[g], varying casting speed and thermocouple temperature break-out system.

3. Oscillation frequency, stroke, drive current and negative strip.

4. The type of steel being cast, on-line composition analysis of the steel[g].

2.2.1.2 Longitudinal cracking (defect 1b)

The occurrence of longitudinal cracks is definitely also widespread across the world, since there is so much literature available on the subject.

Longitudinal cracks are generally caused by improper mould design and condition, high teeming temperature, fast or uneven cooling of the product in both the mould and secondary cooling zone, withdrawal speed and steel composition.

Leclerc and Pollak [77, p. 127] state that "A crack will occur when the strains exceed the resistance of the primary grains to rupture. Shrinkage strains are at a maximum along the axis of the slab and increase with size. Longitudinal full face cracks therefore affect large slabs more and are mainly situated on the axis. Any frictional irregularity between ingot mould and slab dangerously increases local strains, so that the condition of the surface and section of the mould are very important."

The occurrence of the defect is generally more prevalent for wide slabs [53]. The article also states that varying casting speed, irregular or uneven water cooling in the mould, mould oscillation and mould powder are causes of the defect.

Hunter, Madill, Scoones, Hewitt, and Stewart [78] assert that a change of $10 - 15°C$ on thermocouple readings would indicate the formation of a longitudinal crack, so that longitudinal temperature gradients and zero cross points should be considered. Also see Humphreys, Madill, Ludlow, Stewart, Thornton, and Normanton [79], Nakajima, Hiraki, Kawamoto, and Kanazawa [80] and Kang, Lee, Shin, Yang, Lee, Choi, and Lee [81].

Kim, Yeo, Oh, and Lee [82] state that, at a given carbon content, the possibility of longitudinal surface cracking increases with increasing sulphur content[h].

[g] not measure on-line

[h] Moiseev, Esaulov, Nikolaev, Emel'yanov, and Gubin [83] state that a sulphur content of less than 0.02% reduces the risk of longitudinal cracking.

Longitudinal corner cracks Longitudinal corner cracks are defined by Newton *et al.* [59, p. 2] as a crack on the radiused or chamfered part of the section running in the direction of the axis of the product. An example of the defect is given in Fig. 2.5. Mould wear or

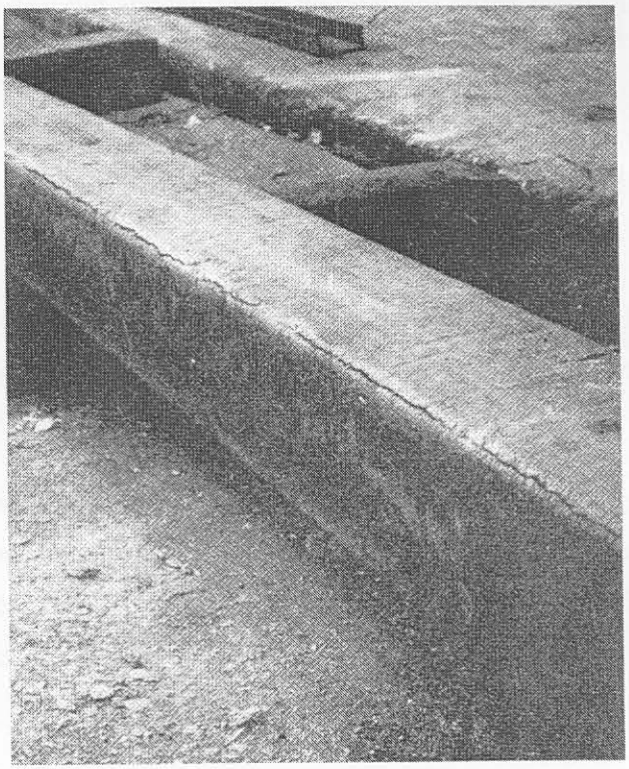

Newton *et al.* [59, p. 2]

Figure 2.5 Longitudinal corner crack.

distortion can cause longitudinal corner cracks, as can uneven mould cooling [59].

Fig. 2.6 taken from Schrewe [1] shows the formation of corner cracks due to shell withdrawal from the heat extracting mould wall for different cross sections. The author states that the gap formed due to the retraction is filled with gas and air. These gases affect the heat transfer efficiency, which means that the heat transfer is uneven which is in turn responsible for uneven solidification. The non-contacting area of the strand undergoes re-heating. This process continues until the strand is strong enough to support the forces of the ferro-static pressure. These expansions and retractions could force the formation of longitudinal corner cracks. The effect of mould taper reversal owed to distortion or wear can also cause these cracks [84]. High tundish temperature & high casting speed are also causes for the formation of the defect. Also, 0.17–0.25% carbon with sulphur$>0.035\%$ or phosphorus $>0.035\%$ are common denominators for the occurrence of the defect [84] in carbon steels.

Saito *et al.* [76] determined that mould level control also has a predominant effect on the

formation of the cracks (see also the paper by Humphreys *et al.* [79]). Large mould level variations can cause depressions which in turn can lead to the formation of longitudinal corner cracks. They further state that mould level variations below 3mm will be adequate to ensure that the defect will not appear due to fluctuations at the meniscus.

Longitudinal facial cracks These cracks are described by Newton *et al.* [59, p. 3] as "a crack not on the radiused or chamfered part of the section, running in the direction of the axis of the product".

Gray *et al.* [70] report that carbon levels in the region of 0.12% ensure that an increase in the occurrence of the defect will result. Specifically, values outside the range of between 0.05% and 0.2% seem to yield very few defects.

Fig. 2.7 shows the relation between casting speed and the occurrence of the defect. This graph indicates that both high or low casting speeds can cause the defect, and that it is solely dependent on the used casting powder's viscosity [70]. Gray *et al.* [70] also state that the origin of the defect is in the mould and that excessive cooling in the mould could result in the defect.

Cracks are generally more prevalent for 2% manganese in aluminium-manganese alloys, 0.3% silicon in aluminium-silicon alloy and 15% zinc in aluminium-zinc alloys [85].

Heard and McLean [84] state that carbon levels higher than 0.12% with an increase in sulphur and a decrease in the Mn/S ratio could cause facial cracks. Similar comments are made by Malinochka, Moiseeva, Esaulova, Esaulov, and Shmelev [86]. High or varying casting

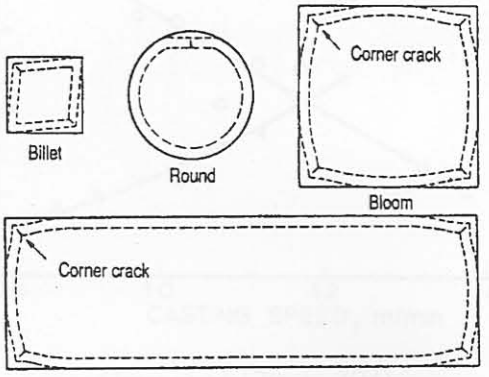

Schrewe [1, p. 106]

Figure 2.6 Gap formation and change in cross section resulting from shrinkage in the mould.

speed also has an influence on the occurrence of the defect. Furthermore, high pouring temperatures, improper mould cooling, taper loss, irregular mould oscillation, mould powder (see *e.g.* Kawamoto, Tsukaguchi, Nishida, Kanazawa, and Hiraki [87]) and a worn mould are also responsible for the defect. The defect seems to be prevalent in large cross sections such as wide slabs.

The occurrence of mid-facial cracks is a consequence of a ductile-brittle transition temperature in the mould possibly with the added effect of mould powder inclusion within the crack [55]. There is non-uniformity in cooling within the mould known as hot-spots which are caused by either uneven mould flux distribution or air gaps and therefore originate at the meniscus. Brimacombe *et al.* [55, p. 225] further state that "Under the influence of the thermally generated tensile strains, the crack will open initially close to the solidification front in the high-temperature region of low ductility within the hot spot. If the region is several millimeters beneath the slab surface, the surface, being cooler, will be below the ductile-brittle transition temperature and, therefore, will behave in a ductile manner. In this condition the surface in the vicinity of the hot spot will 'neck', while the interior of the shell in the non-ductile region is separating to form a crack...". This implies that the thermocouple temperature may show an increase due to the hot spot which might indicate the formation of the defect.

Fig. 2.8 from Irving and Perkins [88] shows the percentage of good slabs (*i.e.* slabs without any defects present) occurring versus % carbon, Mn/S ratio and % sulphur for carbon steels.

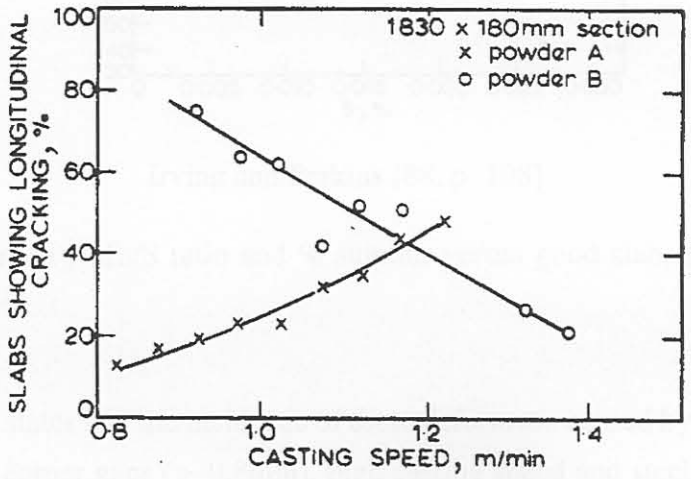

Gray *et al.* [70, p. 304]

Figure 2.7 Longitudinal facial cracking as a function of casting speed for different casting powders.

This figure shows that steels with a carbon content of 0.12% are most prone to the defect. The same can be said for low Mn/S ratios and high sulphur content. The incidence under these circumstances is higher for low casting speeds (large cross sections) than for fast casting speeds (small cross sections). Table 2 in Irving and Perkins [88] also indicates that faster casting speeds—even with large cross sections—seem to show a decrease in the appearance of the defects. The quality of the cast slab is sensitive to the type of mould powder used, especially in cases where mould oil is the flux agent [69]. The paper by Brimacombe and

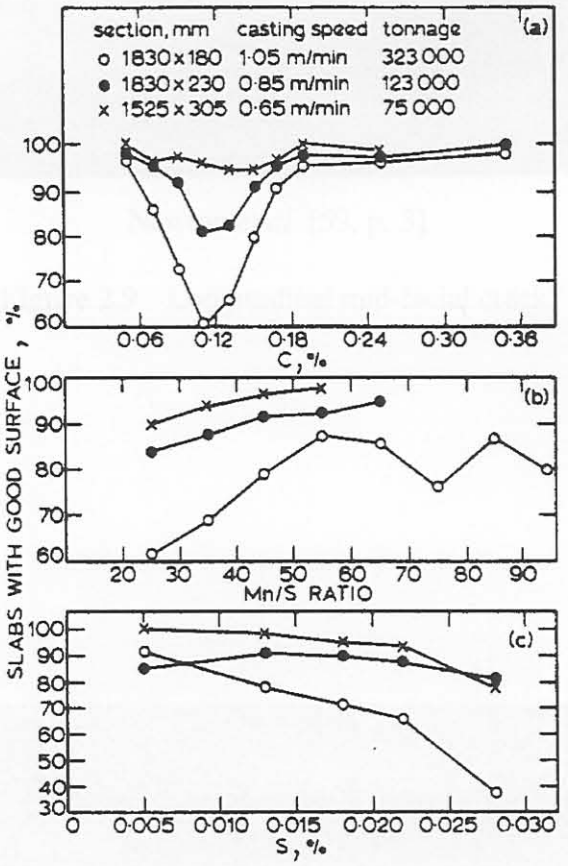

Irving and Perkins [88, p. 108]

Figure 2.8 % carbon , Mn/S ratio and % sulphur versus good slabs (longitudinal facial cracks) in carbon steels.

Samarasekera [50] states that the incidence of these defects are caused by mould taper reversal in billets, high corner gaps (> 0.8mm), high casting speed and steel containing 0.17 to 0.25% carbon, sulphur levels lower than 0.035% and a phosphorus composition higher than 0.035% in carbon steels.

There are two categories, mid-facial (Fig. 2.9) and "near to the corner" (Fig. 2.10) longitudinal facial cracks.

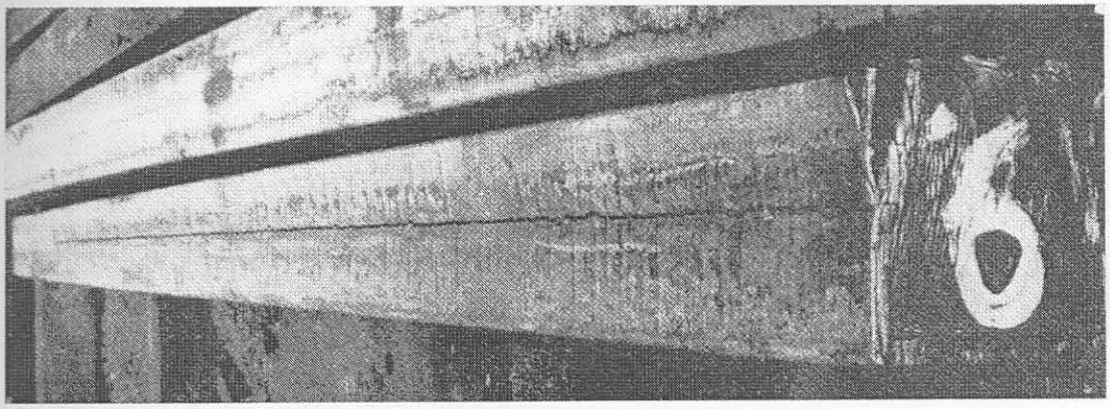

Newton *et al.* [59, p. 3]

Figure 2.9 Longitudinal mid-facial crack.

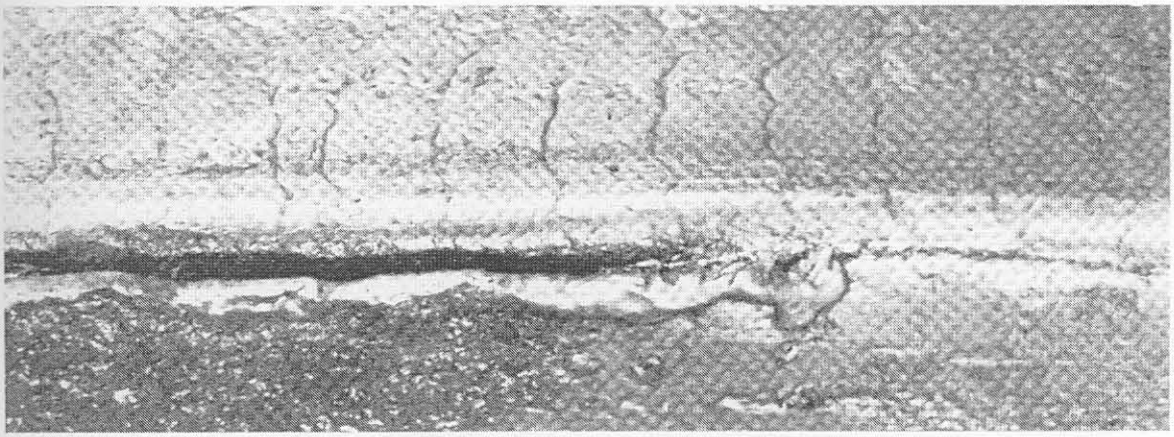

Newton *et al.* [59, p. 4]

Figure 2.10 Longitudinal "Near to the Corner" facial crack.

Discussion The formation of longitudinal cracks in the case of the industrial partner seems to be minimal since the defect occurs on very few slabs.

For the purpose of this thesis, it will be wise then only to consider the formation of longitudinal facial cracks as a whole as described in literature. Based on literature, it seems that facial cracking is more prevalent than corner cracking. The occurrence of facial cracking is due to the following mould conditions:

1. Improper mould design and condition.
2. High teeming (pouring) temperature.
3. Fast or uneven cooling in the mould.
4. Withdrawal speed.
5. Steel composition.
6. Frictional irregularity, *i.e.* wrong taper.
7. Cross sectional size.
8. Mould oscillation.
9. Mould level.

The occurrence of mould level control (point 9) was the only parameter which did not feature in the literature as a probable cause for the occurrence of longitudinal facial cracks, but was investigated anyway. The mould parameters which could indicate the above mentioned abnormal operating conditions are (by point number)

1. Off-line copper mould inspection.
2. Thermocouple measurements.
3. Thermocouple measurements as well as computed longitudinal and transversal gradients. Mould temperature pattern. Average heat flux. Water inlet temperature and flow.
4. Casting speed fluctuations/ abnormalities.
5. Metallurgical evaluation of steel off-line.

6. Evaluation of casting powder.
7. Stroke length, oscillation frequency and negative strip.
8. Mould level and mould level control.

Naturally, the off-line inspected parameters will be obtained too late to be used in a forecasting system.

2.2.1.3 Inclusions (defects 2a & 2b)

The incidence of surface inclusions falls under the category *cleanliness* as described in §2.2.1 on page 14. From the available literature, it seems that inclusions are difficult to detect online because the formation of these defects using abnormal mould parameter perturbations is not discussed.

Newton *et al.* [59] describe inclusions under *entrapped scum* and *carburization*, while the personnel at the industrial partner specifically define their inclusions as *casting powder entrapment* (defect 2a) and *other inclusions* (defect 2b). The term *entrapped scum* is meant to reflect products of de-oxidation or of refractory erosion that are trapped at the meniscus, forming patches at the strand surface, or of slag particles that are entrapped. *Carburization* specifically indicates the localised pickup of carbon from improper lubricating oils or powders (see Fig. 2.11 and also McPherson and McIntosh [89]). This specifically happens

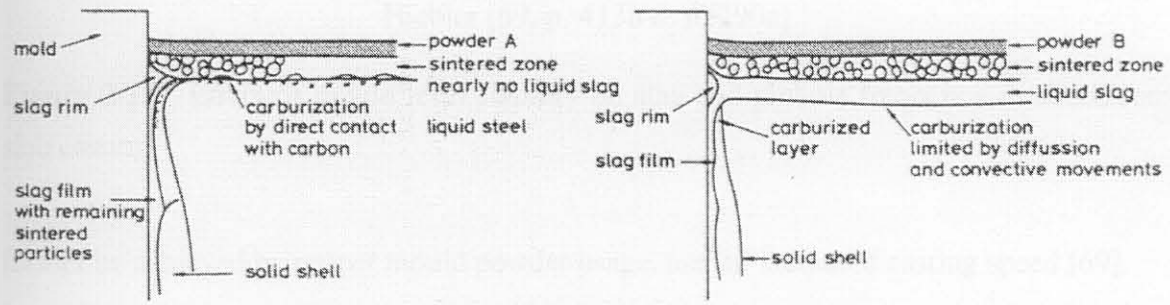

Hiebler [69, p. 405b & p. 284a]

Figure 2.11 Carburization for the case of insufficient (powder A) and sufficient (powder B) liquid slag layer thickness in continuous slab casting of SUS 321 grade.

in low-carbon stainless steels. The defect can commonly only be detected by micro examination or examination of the pickled rolled product. *Casting powder entrapment* is the

inclusion which results specifically from improper powder addition or improper powder type and bad mould level control and can also cause other defects (see §2.2.1.1). *Other inclusions* is understood to describe all other possible inclusions, be it from improper slag outflow in the tundish, refractory de-oxidation or de-oxidation of any non-metallic inclusion in the steel [90].

Due to the low incidence of articles describing the defects under *casting powder entrapment* or *other inclusions*, the available literature found on inclusions in general will be described under one heading.

Hiebler [69] state that a highly stable mould level is the most vital prerequisite in minimising slag inclusion and pinhole occurrence (Fig. 2.12). Also, the minimisation of the defect can

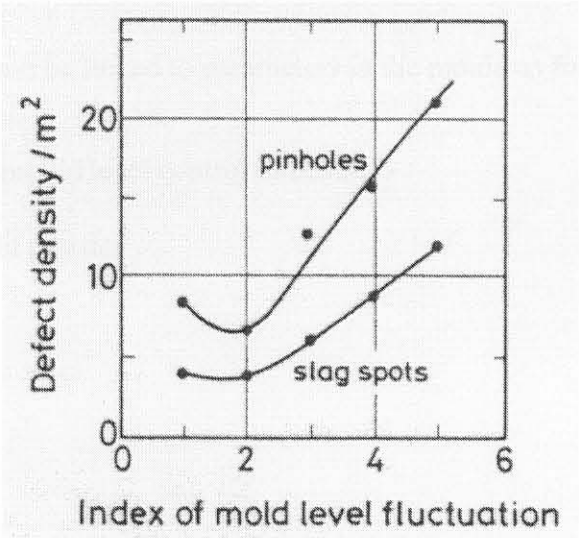

Hiebler [69, p. 413b & p. 290a]

Figure 2.12 Effect of mould level stability on slag and pinhole frequency in continuous slab casting.

further be achieved by proper mould powder usage, and an increased casting speed [69].

The casting powder which is used is in itself responsible for the absorption of other inclusions [91]. This implies that the effect of improper mould powder usage is two-fold. Firstly, the mould powder itself becomes an inclusion and secondly, the mould powder will not absorb other impurities, meaning that inclusions will result. The correct mould powder and mould powder usage are therefore essential as an initial step in the prevention of inclusions[i].

[i] see also Mills, Grieveson, Olusanya, and Bagha [92], Mills [93] and Soares, Fonseca, Neuman, Menezes, Lavinas, and Dweck [94] for detailed discussions on mould powder usage.

The article by Nuri *et al.* [52] states that it is difficult to determine the amount of inclusions by conventional methods such as printing paper analysis[j] when the slab surface roughness increases considerably. This implies that inclusions can be even more difficult to detect when an on-line system such as an optical slab surface inspection system or inspections by humans are used.

From the above discussion, it is clear that inclusions are caused by the following:

1. Bad mould level control.
2. Improper mould powder or mould powder usage.
3. Improper nominal casting speed or casting speed variations.

The above can once again be linked to parameters in the mould as follows:

1. Mould level and mould level control indicator.
2. Analysis of mould powder[k].
3. Casting speed.

2.2.1.4 Sticking

The occurrence of *sticking* or *stickers* was not investigated by the author because the test slabs which were available did not have the defect on any of them (0% occurrence). This is due to the fact that the slabs which did have the defect were probably scrapped. The defect will however be discussed because of its close relation to bleeder defects.

Stickers are generally caused by a hot spot forming at the surface of the strand, which, together with improper mould powder usage, cause the strand to *weld* itself to the copper mould surface. In severe cases, the shell ruptures below the mould causing the molten steel to flow out of the hole in the thinned strand shell. This destructive phenomenon is known as a *break-out*[l]. In less critical situations, the slab skin may repair itself by re-solidification at the mould wall with no sticking so that a *bleeder* occurs (see §2.2.1.5).

[j] A thin layer of *e.g.* gold or sulphur is deposited onto paper. The paper is then adhered to the slab surface where protruding inclusions make imprints on the deposit. The paper is then examined under a scanning electron microscope to investigate the defects.

[k] this is generally not feasible on-line

[l] see *e.g.* Savage and Pritchard [95]

The occurrence of an impending break-out is easily detected by thermocouples arranged as rows down the mould. An increase in thermocouple readings close to the meniscus coupled with an increase in thermocouples further from the meniscus after a period of time is usually an indication of the impending break-out and corrective action such as casting speed reduction can be made [17, 71, 96, 97].

Due to the unavailability of test slabs with the relevant defect, the literature—which is ample—will not be discussed within this thesis.

2.2.1.5 Bleeding (defect 4)

A *bleed* is defined by Newton *et al.* [59, p. 9] as "Exudation of molten metal through a rupture in the skin".

Hiebler [69, p. 285a] states that "Liquid steel may penetrate until re-solidification takes place at the mould wall, *i.e.* , 'bleeding', 'false wall', or 'double skin', and, if steel flow is not stopped, result in a break-out...". The bleeder is thus a "recovered" or re-solidified sticker [98]. Examples of the defect are given in Fig. 2.13 and Fig. 2.14. Kumar, Walker,

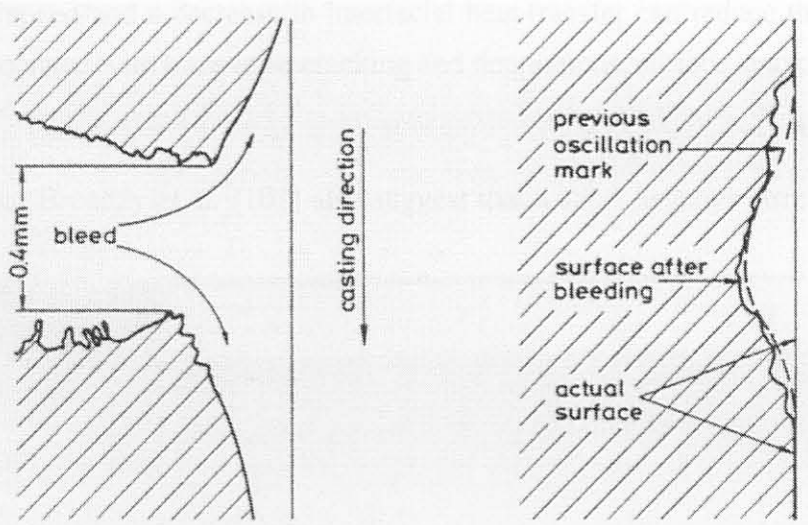

Hiebler [69, p. 406b&p. 285a]

Figure 2.13 Schematic depicting occurrence of *bleeding* in continuous casting

Samarasekera, and Brimacombe [99] determined that uneven oscillation marks are associated with the occurrence of bleeds, especially in the case of billets. The defect occurs close to the meniscus, and due to the relation of the defect to uneven oscillation marks, the defect

is also associated with depressions. The authors further say that the occurrence of the defect can be detected by periodic decreases (known as *valleys*) in the thermocouple readings.

2.2.1.6 Oscillation marks (defects 5a & 5b)

Oscillation marks are caused by the oscillating action of the mould. The defect is a *shape* problem as defined under point 4 in §2.2.1. An example of an oscillation mark is given in Fig. 2.15, and the formation mechanism is shown by Bobadilla, Jolivet, Lamant, and Larrecq [100] in Fig. 2.16. The defect is usually "... separated by a distance related to the amount the product has ascended in one cycle of the reciprocation" in the longitudinal direction [59, p. 14]. The heavy/deep oscillation mark can lead to *skin drag*, characterised by *longitudinal displacement* of part or parts of the reciprocation marks. This is assumed to indicate an uneven oscillation mark.

The defect is almost always present to some degree on the surface of the strand. The oscillation marks are sometimes due to cyclic rupturing and re-welding of the strand surface [69]. A long "time of heal" is required to ensure that the defect is a minimum. This can be achieved by short strokes and high cycle frequency (short negative strip time). Also, high superheat and/or casting speed and a decrease in interfacial heat transfer can reduce the defect. The defects are associated with transverse cracking and depressions, surface cracks and pinholes [101].

Schrewe [1] and Brendzy *et al.* [101] also suggest that a short negative strip time together

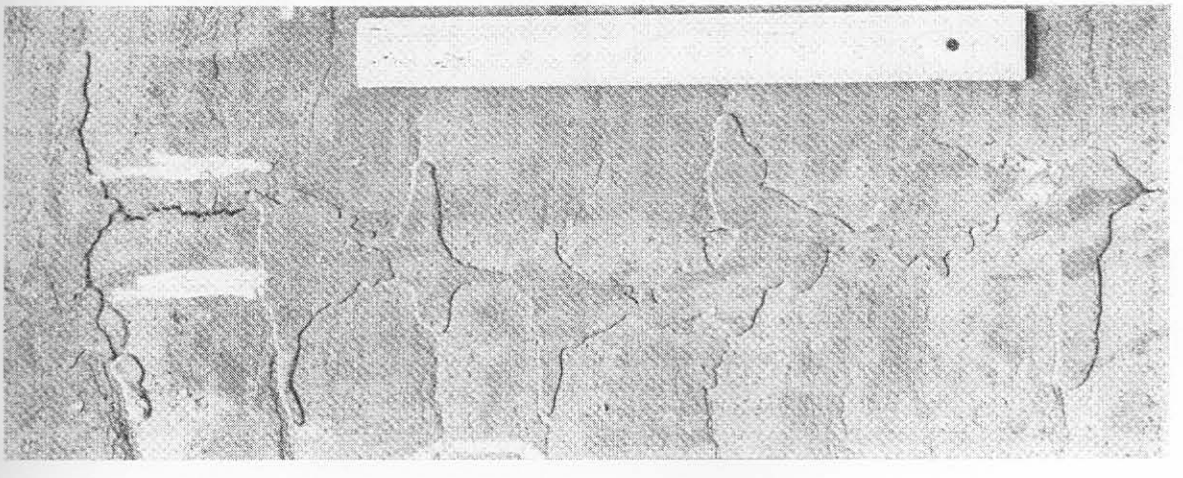

Newton *et al.* [59, p. 9]

Figure 2.14 Occurrence of a bleed in a continuously cast slab.

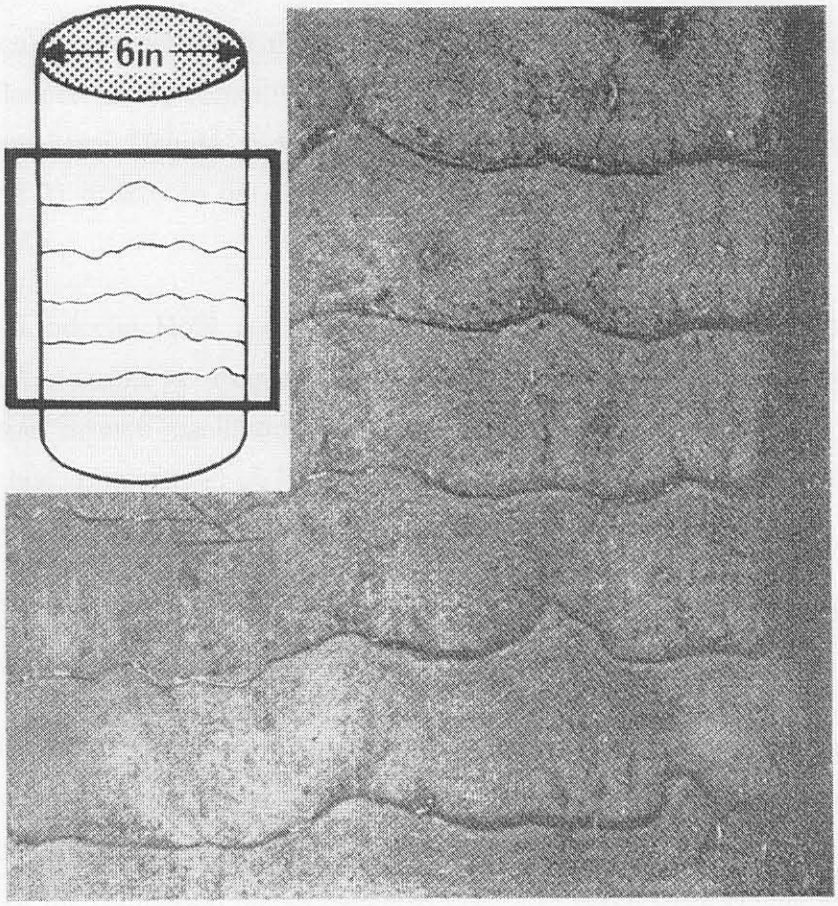

Newton *et al.* [59, p. 14]

Figure 2.15 Oscillation marks on a round.

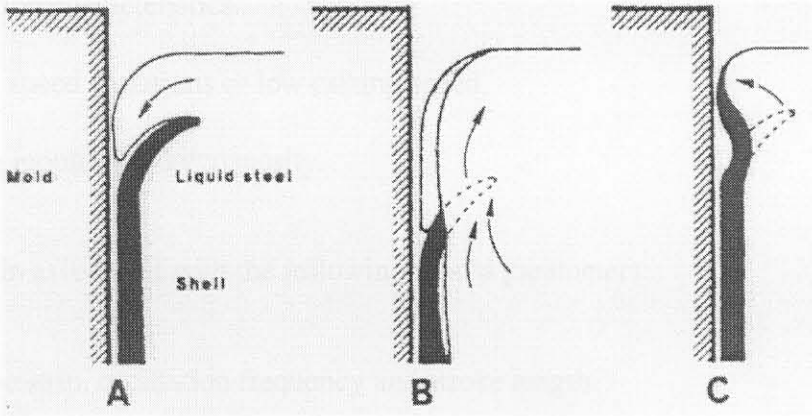

Bobadilla *et al.* [100, p. 277]

Figure 2.16 Three main mechanisms for the formation of oscillation marks in billets: A. overflow; B. overflow + remelting; C. meniscus bent back.

with carbon content control in the steel decreases the occurrence of the defect. The *stiffness* of the meniscus is controlled by the composition of the steel and can therefore also have a positive influence on the formation of oscillation marks. In contrast, Suzuki, Mizukami, Kitagawa, Kawakami, Uchida, and Komatsu [102] state that the 1) shape of the oscillation frequency, and 2) stroke, do not seem to have a remarkable effect on the severity of the oscillation marks.

The article by Lindorfer, Hödl, and Mörwald [103] shows that the conventional mould oscillation method[m] of stroke *vs.* frequency as a function of casting speed requires more mould powder than the "inverse" oscillation method[n]. The industrial partner currently uses the conventional method. Lindorfer *et al.* [103] also state that in their study, they could not find any relation between negative strip time and oscillation mark depth.

Szekeres [65] also states that the oscillation mark is a region where transverse cracking could occur (see also §2.2.1.1).

The effects of casting speed and negative strip time on oscillation mark depth for different carbon levels can be found in the articles by [91, 104]. High casting speed decreases the severity of the defect. A short negative strip time seems to have the same type of effect on the depth of the oscillation marks (see also Fig. 2.17 taken from Hague and Parlington [105]). The oscillation marks can be divided into deep oscillation marks (defect 5a) and uneven oscillation marks (defect 5b), but no literature was found to describe each defect separately. The main causes of the defects are

1. Oscillation characteristics.
2. Casting speed variations or low casting speed.
3. Varying mould powder viscosity.

These are again associated with the following mould parameters:

1. Negative strip, oscillation frequency and stroke length.
2. Casting speed.
3. In-mould flux viscosity.

[m] stroke remains constant and frequency increases with increasing casting speed
[n] stroke increases as frequency decreases with increasing casting speed

2.2.1.7 Stopmarks (defect 6)

The stopmarks defect was not found in the literature, but occurs when there is an abrupt slow-down in the casting procedure. A stopmark is defined as "a band-like pattern around the full perimeter of an extruded section and perpendicular to its length. A stop mark occurs whenever the extrusion process is suspended" [106].

Though no literature was found on the subject, stopmarks will be investigated, as they occur on slabs cast by the industrial partner.

2.2.1.8 Depressions (defect 8)

Depressions are one of the most frequently occurring surface defects at the industrial partner.

Depressions fall under point 4 in §2.2.1. They are divided into transversal and longitudinal depressions. Longitudinal depressions are linked to longitudinal cracks and are narrow sunken areas along the length of the strand. Transversal depressions are caused due to a lack of contact to the mould wall and show up as a sunken area along the transversal section of the

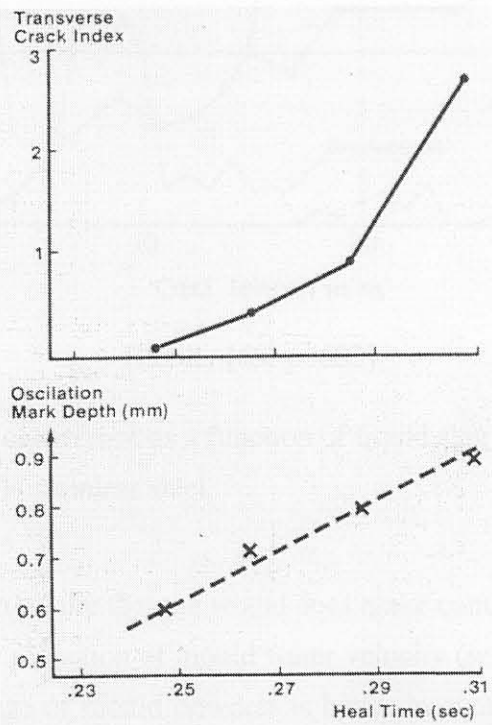

Hague and Parlington [105, p. 37]

Figure 2.17 Effect of heal time on oscillation mark depth.

strand. This lack of contact is generally due to improper mould powder usage or too rapid cooling. The defect can lead to transversal facial cracking (§2.2.1.1), bleeding (§2.2.1.5) or break-outs (§2.2.1.4) [59].

Chandra, Brimacombe, and Samarasekera [107] state that mould taper reversal and mould distortion as well as carbon content of the steel could influence the occurrence of the defect.

The first slab cast also has the most depressions [104, 108, 109] while slabs that follow are less prone to the defect.

Transversal depressions Hiebler [69] state that transversal depressions result from a non-uniformity (unevenness) in the shell growth, and that the effect of carbon is quintessential in the formation thereof. The effect of mould powder used shows from Fig. 2.18 that depression formation decreases as the molten slag layer increases. This once again shows that proper usage of mould powders is very important for the prevention of several defects. A remedy

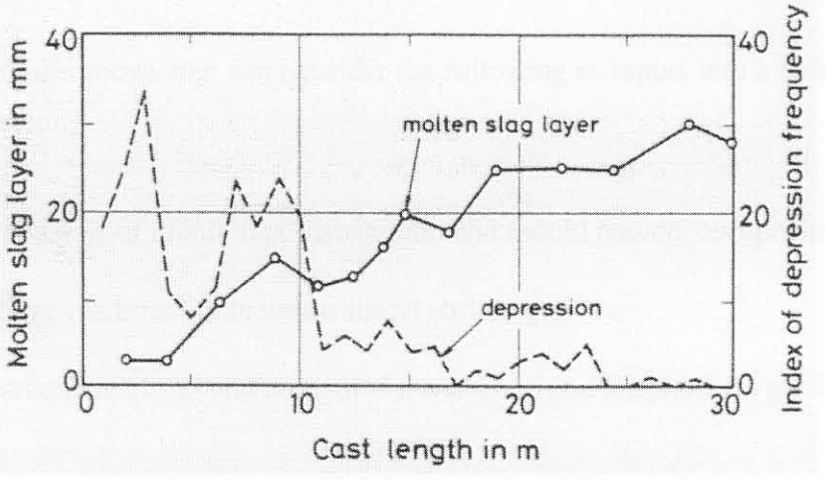

Hiebler [69, p. 603]

Figure 2.18 Depression occurrence as a function of liquid slag layer thickness in continuous slab casting of SUS 304 stainless steel.

is the use of *soft cooling* to ensure that the strand does make contact with the mould surface. This could be done by the reduction of mould water velocity (see *e.g.* Wolf [110] and Wolf [111]), but the proper usage of mould powders is better in controlling mould-slab surface contact [69].

Longitudinal depressions Longitudinal depressions are very closely associated to longitudinal cracking, and hence their causes are similar. See §2.2.1.2. Longitudinal off-corner depressions occur due to improper usage of mould powder and too rapid cooling together with improper mould taper at the corner of the slab so that the strand shrinks away from the mould [91].

Discussion The occurrence of the defect will not be treated under the two sub-depression headings. The formation of the defects are generally due to:

1. Mould powder.
2. Mould taper and distortion.
3. Too rapid cooling in the mould or secondary cooling zone.
4. Mould-shell contact.

Associated with the above, one can consider the following as inputs into a defect prediction and control system:

1. On-line analysis of mould flux distribution and mould powder composition.
2. Strain gauge readings[o] to measure strand shrinkage.
3. Thermocouple readings and computed *transversal* and longitudinal gradients.

2.2.1.9 Defect summary

Table 2.1 shows a summary of the general causes for defects based on the literature in the previous sections. It is interesting to note that most authors do not explicitly link mould level to defects, with only longitudinal cracking and inclusions being explicitly mentioned. Contrary to this, researchers address the mould level control problem as the most important single factor that contributes to surface defects (see §2.2.1). However, every considered defect is linked by the literature to some variable in the mould. The mould is therefore quintessential in the formation of defects.

[o]not use at the industrial partner

Table 2.1 Summary of causes for defect occurrence based on the literature review. An "•" indicates that the variable in question has an influence on the defect. Bold variables can be measured on-line.

	Transversal cracking (1a)	Longitudinal cracking (1b)	Inclusions (2a & 2b)	Bleeders (4)	Oscillation marks (5a & 5b)	Stopmarks (6)	Depressions (8)
Mould level		•	•				
Mould powder	•	•	•		•		•
Mould friction	•						
Mould taper	•	•					•
Mould oscillation	•	•	•		•		
Casting speed	•	•	•		•	•	
Temperature	•	•		•	•		•
Composition	•	•			•		•
Tundish			•				
Superheat					•		
Bending	•						

Another important point to note from the literature is that strand temperature plays a role in all the defects except inclusions and stopmarks. This suggests that temperature is a very valuable variable to use in any type of defect predictor.

Mould powder and mould friction are very closely related and are difficult to measure on-line, as is the taper of the mould [112].

Composition is a factor which does not change dynamically during casting. However, the composition of some steels is a factor that is influential in the formation of certain defects.

Measurement of inclusion outflow in the tundish is also difficult to quantify on-line and superheat is generally not measured at regular intervals (see *e.g.* Ozgu [112]).

2.2.1.10 Defect models

Some literature exists on the modelling of defects. Chipalo, Gilchrist, and Smith [113] and Gilchrist and Smith [114] show results of a finite element technique to model the *propagation* of cracks. The actual model is not presented and no relation to casting variables are given.

Kametani [115] gives a method to determine the frequency distributions of longitudinal crack length and frequency. Again there is no relation to casting variables. Hunter *et al.* [78] speak of a prediction algorithm based on a exponential smoothing technique which uses a non-weighted average of previous temperature values to predict temperature in the mould, and according to the difference between the actual and predicted temperatures decide whether a longitudinal crack will occur or not. The model is not presented and accuracies of up to 80% for longitudinal cracks longer than 400mm have been achieved. Hunter *et al.* [18] use artificial neural networks to predict longitudinal depressions and cracks. For stainless steel, they predict 61.5% of the longitudinal cracks accurately.

De Santis and Ferretti [116] mathematically describe the path that an inclusion takes from the tundish through the SEN into the liquid pool. The use of the model to predict *surface* inclusions is not described. Bouris and Bergeles [117] describe a model to *track* an inclusion which travels to the slag-steel interface, thus being able to remain there to be trapped at the surface to form a surface inclusion. The application of the model to predict when inclusions will occur at the surface, based on plant parameters, is not made. Sawada, Takeuchi, Tanaka, Okazawa, and Shigematsu [118] also describe a model to track inclusions inside the mould from the SEN output, but do not explain how the model can be used to predict surface inclusions based on process parameters, Yamada, Fukumoto, Tanaka, Matsumiya, and Wajima

[119] describe the size distribution and amount of particles inside the liquid pool, but do not give the actual model nor its relationship to casting parameters. McDavid and Thomas [120] give a model to determine the behaviour of the slag/flux at the meniscus, sometimes causing a concentration of flux near the surface which may cause quality problems. Bailey, Chow, Cross, Fryer, and Pericleous [121] give detailed models and model simulations for inclusions and porosity in ingot-type moulds. This has however not been extended to continuous casting.

Henriksen, Jensen, and Mortensen [122] describe a simulation package for bleeder modelling, but do not show the model in the paper.

King, Lacey, Please, Willmott, and Zoryk [123] present a model to describe the formation of oscillation marks but state that only initial results of the model are available. Sha, Diedrichs, and Schwerdtfeger [124] present a model to describe the behaviour at the liquid/liquid interface of steel and slag during oscillation motion. This theory can possibly be used to derive a model for oscillation mark formation.

Thomas, Moitra, and Zhu [125] and Thomas, Moitra, and McDavid [126] describe the use of a coupled finite element model to model the thermo-mechanical behaviour of a thin slice as it moves through the caster. This model is then applied to longitudinal depression investigations. The model is however not given.

Thomas, Lui, and Ho [127] give a model for transversal depressions, and describe their effect of heat transfer in the mould. The authors state that "These results should be useful in the difficult task of interpreting transient mold thermocouple signals for on-line quality monitoring".

Gugliermina, Codur, and Cardouat [128] discuss models to predict defects but do not state what type of models are used, nor give results of the accuracy of the models. The same can be said of the paper by Irving [129].

Short, Barber, Normanton, Patrick, and York [130] discuss models to predict surface temperature in the mould, but do not present the model and do not indicate whether the outflow from the SEN is included in the model.

Some other types of models may aid in an eventual first principles model for defects. Royzman [131] gives a model describing friction in the mould. O'Malley [132] gives a description of transient temperature behaviour in the mould. Matsumiya, Ohashi, and Abe [133] give a model of thermal stress that result from the bending and unbending of the strand. Li and Ruan

[134] give a model of thermal stresses and temperature during aluminium casting. Lamant, Larrecq, Birat, Hensgen, Weber, and Dhuyvetter [135] give a model of slab bulging. Harste, Deisinger, Steinert, and Tacke [136] give a thermal and mechanical model of the entire casting process. Das and Sarkar [137] give a control volume approach to thermal modelling in continuous casting. Breslin, Hetherington, and Walker [138] speak of models for high temperature materials, air gap formation, ferro-static loading, flux heat transfer and mould taper, but do not actually give the models. Lastly, Camisani-Calzolari [35] gives a thermal model and optimisation procedure for the secondary cooling zone.

The preceding explanation of literature described the causes of defects in the continuous casting process. Table 2.1 gives a summary of the causes of the defects. First principle models of defect propagation and prediction have been found in literature, but do not give the mathematical models in the papers or are not suitable for predicting defects based on process variables. The derivation of a first principle model falls outside the scope of this work.

2.2.2 Goodness-of-fit tests

In certain situations such as encountered in this thesis, it is necessary to perform a statistical hypothesis test that determines whether an independent random variable, X_1 belongs to the same distribution as another random variable, X_2. Such tests are known as goodness-of-fit tests [139].

Goodness-of-fit tests determine whether a sample of values (which make up an empirical distribution) come from a given theoretical distribution. With enough data, the distribution of *e.g.* X_2 can be thought of as the "theoretical distribution". X_1 can then be seen as the "empirical distribution". The hypothesis test then determines whether the empirical distribution (distribution of X_1) comes from the theoretical distribution (distribution of X_2). X_1 can be the mean value of a parameter in the mould on slabs where defects occur, and X_2 can be the mean value of the same parameter on slabs where defects do not occur. In such a case, if the distributions of X_1 and X_2 are similar, then that parameter may not have any effect on the formation of the defects.

One of the oldest of these tests is the χ^2-test [140], but more recent tests such as the Kolmogorov-Smirnov and Anderson-Darling tests are more accurate in the outcome of the hypothesis decision [140], and will be used in the remainder.

2.2.2.1 Background

Assume that X is a statistically independent random variable with a probability density function given by $f(x)$, and its cumulative density function is given by

$$F(x) = \int_{-\infty}^{x} f(x)dx. \tag{2.1}$$

The cumulative density function can be directly approximated from the observation values of the sample. Assume that x_i denotes the i-th observation of the random variable X, and that there are n observations. The probability density function can then be *approximated* by a train of Dirac-delta ($\delta(x - x_i)$) functions each with strength $1/n$. The approximation to the probability density function is then

$$f(x) \approx \frac{1}{n}\sum_{i=1}^{n}\delta(x - x_i), \tag{2.2}$$

when there are n observations. To approximate the cumulative density function from the above train of Dirac-delta functions from the probability density function, one can go ahead as follows

$$\begin{aligned} F(x) &= \int_{-\infty}^{x} f(x)dx, && (2.3)\\ &\approx \frac{1}{n}\int_{-\infty}^{x}\left(\sum_{i=1}^{n}\delta(x - x_i)\right)dx, && (2.4)\\ &= \frac{1}{n}\sum_{i=1}^{n}\left(\int_{-\infty}^{x}\delta(x - x_i)dx\right), && (2.5)\\ &= \frac{1}{n}\sum_{i=1}^{n}u(x - x_i). && (2.6) \end{aligned}$$

$u(x - x_i)$ is the unit step function defined by

$$u(x - x_0) = \begin{cases} 1 & x \geq x_0 \\ 0 & x < 0 \end{cases}. \tag{2.7}$$

This idea is illustrated in Fig. 2.19.

2.2.2.2 Kolmogorov-Smirnov test

The first of the goodness-of-fit tests used in this thesis is known as the Kolmogorov-Smirnov test.

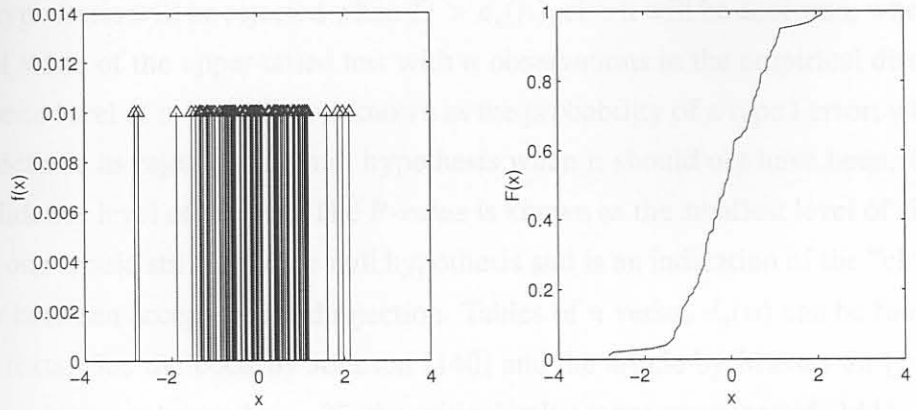

Figure 2.19 Illustration of the effect of using the pulse train probability density function $f(x)$ to determine the cumulative density function $F(x)$ of the random variable X.

Assume that the theoretical cumulative density function is given by $F(x)$ and that the empirically determined distribution is given by $F_n(x)$.

Note that the theoretical distribution is always based on a continuous distribution. The theoretical distribution is usually not continuous, but if there are many observations, the discrete distribution can approximate the continuous distribution approximately *i.e.* the discrete distribution becomes an accurate estimator of the continuous distribution.

The Kolmogorov-Smirnov statistic is given by Massey Jr. [141] as

$$D = max\left|F_n(x) - F(x)\right|, \quad \forall x; \tag{2.8}$$

that is, it is the maximum difference (evaluated at all points of x) of the theoretical and empirical distributions. The null hypothesis (H_0) states that the empirical observations belong to the theoretical distribution. The alternative hypothesis (H_1) states that the two distributions do not belong to the same distribution, *i.e.* they are different.

Rejection of the null hypothesis is a *strong conclusion* and acceptance of the null hypothesis is usually a *weak conclusion*. In the case of a weak conclusion, it is advisable to check the probability of making a type II error (β). A type II error is defined as accepting a null hypothesis when the null hypothesis should not have been accepted and is related to the

power of the test through $\mathcal{P} = 1 - \beta$. The Kolmogorov-Smirnov test has weak power (*i.e.* β is large) [140].

The null hypothesis will be rejected when $D > d_c(n)$, else it will be accepted, where $d_c(n)$ is the critical value of the upper-tailed test with n observations in the empirical distribution at a significance level of $\alpha = 0.05$. α is known as the probability of a type I error; where a type I error is defined as rejecting the null hypothesis when it should not have been. $\mathcal{C} = 1 - \alpha$ is the confidence level of the test. The *P-value* is known as the smallest level of significance for which one would still reject the null hypothesis and is an indication of the "closeness" of the border between acceptance and rejection. Tables of n versus $d_c(n)$ can be found in most statistical texts. See the book by Johnson [140] and the article by Massey Jr. [141]. When observations increase beyond $n = 35$, the critical value takes on values of [141]

$$d_c(n) = \frac{1.36}{\sqrt{n}}, \quad \forall n > 35. \tag{2.9}$$

Also, with $\mathcal{P} = 0.95$ and $\mathcal{C} = 0.95$, the maximum detectable difference of the cumulative distributions is given by $\Delta = 2.2/\sqrt{n}$ [141].

2.2.2.3 Anderson-Darling test

As noted in §2.2.2.2, the Kolmogorov-Smirnov test has weak power. It does not have a great ability to detect situations when there is a significant difference between the empirical and theoretical distributions. Furthermore, this deficit is usually found in the tails of a Normal or near-Normal probability distribution. Another test emerged to counter this problem, and though well documented, is not as well known. The test is known as the Anderson-Darling test for goodness-of-fit [140, 142].

The test statistic is a normalized version of the Kolmogorov-Smirnov test and is given by

$$A^2 = \int_{-\infty}^{\infty} \frac{F_n(x) - F(x)}{F(x)(1 - F(x))} dx. \tag{2.10}$$

The computation of the statistic seems complex, but it can be shown that [140]

$$A^2 = -\frac{\sum_{i=1}^{n}(2i-1)[\ln \mathrm{u}_i + \ln(1 - \mathrm{u}_{n+1-i})]}{n} - n, \tag{2.11}$$

where $\mathrm{u}_i = F(x_{(i)})$ is the value of the theoretical cumulative distribution at the i-th largest empirical observation.

The null hypothesis is the same as with the Kolmogorov-Smirnov test. The null hypothesis will be rejected when the statistic is larger than a critical value in the upper-tailed test. This

value is reported by Johnson [140] as $a_c^2 = 2.492$ with $\mathcal{C} = 0.95$ for normal or near-normal distributions. This means that the null hypothesis will be rejected when $A^2 > 2.492$ to strongly conclude that the empirical distribution is not from the theoretical distribution.

Generally, fewer than 10 observations from the empirical distribution can give unreliable results and more than 40 samples are rarely used in the test [139]. The P-value and power of the test is generally distribution specific, and will thus not be considered here.

The statistical tests to determine whether an empirical distribution forms part of a theoretical distribution was described. Probably, the most accurate tests of this type of goodness-of-fit tests are the Kolmogorov-Smirnov and Anderson-Darling tests. The Kolmogorov-Smirnov test has higher accuracy than the Anderson-Darling test at low sample sizes but is weak in the tails of the distribution. The Anderson-Darling test has high accuracy compared to the Kolmogorov-Smirnov test over the whole distribution but is only truly valid for sample sizes between 10 and 40. For these reasons, both tests can be used when goodness-of-fit tests are required and results can be interpreted accordingly. Another example where statistics are used can be found in the paper by Peters, Link, and Heckenthaler [143] who use statistical methods in the form of multivariate analysis of variance (ANOVA) to find plant-wide dependencies of quality on process variables, but who do not give any results.

2.2.3 Correlation

The term correlation refers to that inference where one tries to determine whether a strong linear relation exists between two random variables. When there is weak correlation, the two random variables, X and Y are not necessarily independent from each other, but may have a strong non-linear relation [144].

This technique can be used to determine whether there are strong linear relations between different inputs. For example, Ikäheimonen, Leiviskä, Russka, and Matkala [145] show how correlation can be used to find the relation between nozzle clogging in the mould and process parameters.

The basic correlation analysis is performed using the correlation coefficient (normalized covariance), and is given by [140]

$$\rho_{XY} = \frac{S_{xy}}{\sqrt{S_{xx}S_{yy}}}, \tag{2.12}$$

where

$$S_{xx} = \sum_{i=1}^{n} (x_i - \bar{x})^2 , \tag{2.13}$$

$$S_{yy} = \sum_{i=1}^{n} (y_i - \bar{y})^2 , \tag{2.14}$$

$$S_{xy} = \sum_{i=1}^{n} (x_i - \bar{x})(y_i - \bar{y}) . \tag{2.15}$$

$\bar{x}$ is the mean value of the random variable X, and x_i is a sample from X. The same can be said about Y. When $|\rho_{XY}| = 1$, there is a perfect linear relationship between X and Y. When $0.75 < |\rho_{XY}| < 1$, there is a strong linear relationship between X and Y *etc.*

2.2.4 Auto regression with exogenous input

This section briefly describes the auto regression with exogenous input (ARX) algorithm and how the model information matrices are calculated (see *e.g.* Ljung [146] for an in depth discussion on this subject.). Firstly, let an $\mathbb{R}^{m\times 1}$ input vector be defined as follows:

$$\mathbf{u}[nT] = \begin{bmatrix} u_1[nT] \\ u_2[nT] \\ \vdots \\ u_m[nT] \end{bmatrix} , \tag{2.16}$$

where $u_i[nT]$ is the i-th input sampled every $t = nT$ seconds at a specific discrete-time described by $n = 0, 1, 2, \ldots, N-1$. Further, define an $\mathbb{R}^{p\times 1}$ output vector as follows:

$$\mathbf{y}[nT] = \begin{bmatrix} y_1[nT] \\ y_2[nT] \\ \vdots \\ y_p[nT] \end{bmatrix} , \tag{2.17}$$

where $y_j[nT]$ is the j-th output at every $t = nT$ seconds at a specific discrete-time described by $n = 0, 1, 2, \ldots, N-1$. The ARX model can then be written as

$$\begin{aligned} \mathbf{A}_0\mathbf{y}[nT] \;+\; & \mathbf{A}_1\mathbf{y}[(n-1)T] + \mathbf{A}_2\mathbf{y}[(n-2)T] + \cdots + \mathbf{A}_{n_a}\mathbf{y}[(n-n_a)T] = \\ \mathbf{B}_0\mathbf{u}[nT] \;+\; & \mathbf{B}_1\mathbf{u}[(n-1)T] + \mathbf{B}_2\mathbf{u}[(n-2)T] + \cdots + \mathbf{B}_{n_b-1}\mathbf{u}[(n-n_b+1)T]. \end{aligned} \tag{2.18}$$

In this realization $\mathbf{A}_0$ is an identity matrix because it is assumed that no outputs influence other outputs at the current discrete-time step. The matrices, $\mathbf{A}_v \in \mathbb{R}^{p\times p}$ are related to the

time-shifted outputs and are defined by

$$\mathbf{A}_v = \begin{bmatrix} a_{1,1}^{(v)} & a_{1,2}^{(v)} & \cdots & a_{1,p}^{(v)} \\ a_{2,1}^{(v)} & a_{2,2}^{(v)} & \cdots & a_{2,p}^{(v)} \\ \vdots & \vdots & \ddots & \vdots \\ a_{p,1}^{(v)} & a_{p,2}^{(v)} & \cdots & a_{p,p}^{(v)} \end{bmatrix} \quad \forall \quad v = 0, 1, 2, \ldots, n_a. \tag{2.19}$$

The $a_{:,:}^{v}$ are constants which ultimately define the output part of the model. Usually, these matrices are diagonal which implies that there is no feedback *i.e.* no outputs influence other outputs directly.

Similarly, the matrices, $\mathbf{B}_w \in \mathbb{R}^{p \times m}$ are related to the time-shifted inputs and are defined by

$$\mathbf{B}_w = \begin{bmatrix} b_{1,1}^{(w)} & b_{1,2}^{(w)} & \cdots & b_{1,m}^{(w)} \\ b_{2,1}^{(w)} & b_{2,2}^{(w)} & \cdots & b_{2,m}^{(w)} \\ \vdots & \vdots & \ddots & \vdots \\ b_{p,1}^{(w)} & b_{p,2}^{(w)} & \cdots & b_{p,m}^{(w)} \end{bmatrix} \quad \forall \quad w = 0, 1, 2, \ldots, n_b - 1. \tag{2.20}$$

The $b_{:,:}^{w}$ are constants which ultimately define the input part of the model.

One can now define the $\mathbb{R}^{pn_a + mn_b \times p}$ system matrix as

$$\Theta = \begin{bmatrix} \mathbf{A}_1 & \cdots & \mathbf{A}_{n_a} & \mathbf{B}_0 & \mathbf{B}_1 & \cdots & \mathbf{B}_{n_b-1} \end{bmatrix}^\top, \tag{2.21}$$

and the data vector of $\mathbb{R}^{pn_a + mn_b \times 1}$ as

$$\psi[nT] = \begin{bmatrix} -\mathbf{y}[(n-1)T] \\ -\mathbf{y}[(n-2)T] \\ \vdots \\ -\mathbf{y}[(n-n_a)T] \\ \mathbf{u}[nT] \\ \mathbf{u}[(n-1)T] \\ \mathbf{u}[(n-2)T] \\ \vdots \\ \mathbf{u}[(n-n_b+1)T] \end{bmatrix}. \tag{2.22}$$

The system in Eq. 2.18 can then be written as

$$\mathbf{y}[nT] = \Theta^\top \psi[nT]. \tag{2.23}$$

However, the system in Eq. 2.23 will give a predictor based on only one time sample. The result is that the predictor will only be able to detect a situation which is exactly similar to the

training set of data. To compensate for this, one needs several samples to define an adequate model. This can be achieved by lumping the different time instance data together and thus forming a predictor which is averaged about all the data. This, in effect, eliminates the time dimension of the system. Thus, define an output $\mathbb{R}^{p\times N}$ matrix as follows:

$$\mathbf{Y}[nT] = \begin{bmatrix} \mathbf{y}[nT] & \mathbf{y}[(n+1)T] & \mathbf{y}[(n+2)T] & \cdots & \mathbf{y}[(n+N-1)T] \end{bmatrix}, \tag{2.24}$$

and a $\mathbb{R}^{pn_a+mn_b\times N}$ data matrix as follows:

$$\mathbf{\Psi}[nT] = \begin{bmatrix} \boldsymbol{\psi}[nT] & \boldsymbol{\psi}[(n+1)T] & \boldsymbol{\psi}[(n+2)T] & \cdots & \boldsymbol{\psi}[(n+N-1)T] \end{bmatrix}. \tag{2.25}$$

The system can now be written as

$$\mathbf{Y}[nT] = \mathbf{\Theta}^\top \mathbf{\Psi}[nT]. \tag{2.26}$$

An estimate of the outputs will be given by

$$\hat{\mathbf{Y}}[nT, \hat{\mathbf{\Theta}}] = \hat{\mathbf{\Theta}}^\top \mathbf{\Psi}[nT], \tag{2.27}$$

where $\hat{\mathbf{Y}}[nT, \hat{\mathbf{\Theta}}]$ is the estimated values of the outputs, based on some specific $\mathbf{\Theta}$, and $\mathbf{\Psi}[nT]$ are past values of the outputs and inputs.

To determine an estimate of the predictor ($\hat{\mathbf{\Theta}}$), a least squares approach can be used. Define the error between the true and predicted outputs as follows

$$\mathbf{\Xi}[nT, \hat{\mathbf{\Theta}}] = \mathbf{Y}[nT] - \hat{\mathbf{Y}}[nT, \hat{\mathbf{\Theta}}], \tag{2.28}$$

for a particular set of time samples. Define the least square error of $\mathbf{\Xi}$ as

$$V(\hat{\mathbf{\Theta}}) = \frac{1}{2}\|\mathbf{\Xi}[nT, \hat{\mathbf{\Theta}}]\|_F^2 = \frac{1}{2}\mathrm{tr}\left(\mathbf{\Xi}[nT, \hat{\mathbf{\Theta}}]^\top \mathbf{\Xi}[nT, \hat{\mathbf{\Theta}}]\right) \tag{2.29}$$

$$= \frac{1}{2}\mathrm{tr}\left(\left[\mathbf{Y}[nT] - \hat{\mathbf{Y}}[nT, \hat{\mathbf{\Theta}}]\right]^\top \left[\mathbf{Y}[nT] - \hat{\mathbf{Y}}[nT, \hat{\mathbf{\Theta}}]\right]\right) \tag{2.30}$$

$$= \frac{1}{2}\mathrm{tr}\left(\left[\mathbf{Y}[nT] - \hat{\mathbf{\Theta}}^\top \mathbf{\Psi}[nT]\right]^\top \left[\mathbf{Y}[nT] - \hat{\mathbf{\Theta}}^\top \mathbf{\Psi}[nT]\right]\right), \tag{2.31}$$

and $\|\boldsymbol{X}\|_F^2$ is the Frobenius norm of $\mathbf{X}$. To determine the minimum least square error, the above expression is differentiated to $\hat{\mathbf{\Theta}}$ and set equal to zero to give the least squares predictor, based on plant input/output data.

$$\left.\frac{\partial V(\hat{\mathbf{\Theta}})}{\partial \hat{\mathbf{\Theta}}}\right|_{\mathbf{\Theta}\to\hat{\mathbf{\Theta}}} = \mathbf{\Psi}[nT]\mathbf{\Psi}[nT]^\top \hat{\mathbf{\Theta}} - \mathbf{\Psi}[nT]\mathbf{Y}[nT]^\top = \mathbf{0}. \tag{2.32}$$

This gives the least square output error predictor

$$\hat{\mathbf{\Theta}} = \left[\mathbf{\Psi}[nT]\mathbf{\Psi}[nT]^\top\right]^{-1} \mathbf{\Psi}[nT]\mathbf{Y}[nT]^\top. \tag{2.33}$$

The least square predictor is then implemented by

$$\hat{\mathbf{y}}_{LS}[nT] = \hat{\Theta}^{\top} \psi^*[nT], \tag{2.34}$$

where $\psi^*[nT]$ is the input consisting of the past predicted outputs and the past and present inputs, since no step-ahead prediction is used:

$$\psi^*[nT] = \begin{bmatrix} -\hat{\mathbf{y}}_{LS}[(n-1)T] \\ -\hat{\mathbf{y}}_{LS}[(n-2)T] \\ \cdots \\ -\hat{\mathbf{y}}_{LS}[(n-n_a)T] \\ \mathbf{u}[nT] \\ \mathbf{u}[(n-1)T] \\ \mathbf{u}[(n-2)T] \\ \cdots \\ \mathbf{u}[(n-n_b+1)T] \end{bmatrix}. \tag{2.35}$$

The preceding discussion has been given to make the terminology clear. To solve the ARX models, the MATLAB system identification toolbox [147] was used.

2.2.5 Linear quadratic tracker at steady-state (LQTSS)

The linear quadratic regulator (LQR) is an optimal state feedback controller used to regulate the state of a system to compensate for disturbances in the system state. The LQR drives the state of a system to zero by manipulation of the inputs.

It is often not the intension to drive the state of the system to zero, but rather to allow the system output to track a reference input [148]. This can be achieved by a linear quadratic tracker (LQT). The LQT is essentially an LQR with a feed-forward path added to the control scheme [148].

The LQT is generated by optimizing a performance index subject to the constraints that the system dynamics impose. A control law, based on the current state of the system as well as future knowledge of the desired reference trajectory is implemented in a feed-forward-feedback scheme. These ideas will be discussed here.

2.2.5.1 State-space model

A multi-input, multi-output (MIMO), linear, time-invariant (LTI) system can be described in state-space by

$$\dot{\mathbf{x}}(t) = \mathbf{A}\mathbf{x}(t) + \mathbf{B}\mathbf{u}(t), \quad \mathbf{x}(t_0) = \mathbf{x}_0 \tag{2.36}$$

$$\mathbf{y}(t) = \mathbf{C}\mathbf{x}(t) + \mathbf{D}\mathbf{u}(t), \tag{2.37}$$

where $\mathbf{x} \in \mathbb{R}^{N_x \times 1}$ is a vector of the N_x states of the system, $\mathbf{y} \in \mathbb{R}^{N_y \times 1}$ is a vector of the N_y outputs of the system and $\mathbf{u} \in \mathbb{R}^{N_u \times 1}$ is a vector of the N_u inputs of the system. $\mathbf{A} \in \mathbb{R}^{N_x \times N_x}$ is the system matrix, $\mathbf{B} \in \mathbb{R}^{N_x \times N_u}$ is the input matrix, $\mathbf{C} \in \mathbb{R}^{N_y \times N_x}$ is the output matrix and $\mathbf{D} \in \mathbb{R}^{N_y \times N_u}$ is the feed-forward matrix [149]. $\mathbf{x}_0$ is the initial condition of the state at time t_0. Assume in this study that the state-space representation can be generated without the use of the feed-forward matrix (*i.e.* $\mathbf{D} = \mathbf{0}$).

2.2.5.2 Linear quadratic tracker

The LQT optimises the performance index

$$J(t_0) = \frac{1}{2}\mathbf{e}^\top(T)\mathbf{P}\mathbf{e}(T) + \frac{1}{2}\int_{t_0}^{T} \mathbf{e}^\top(t)\mathbf{Q}\mathbf{e}(t) + \mathbf{u}(t)\mathbf{R}\mathbf{u}^\top(t)dt, \tag{2.38}$$

where

$$\mathbf{e}(t) = \mathbf{r}(t) - \mathbf{z}(t), \tag{2.39}$$

is the tracking error between the desired performance output, $\mathbf{r} \in \mathbb{R}^{N_s \times 1}$ and the performance output of the system $\mathbf{z} \in \mathbb{R}^{N_s \times 1}$ [148]. N_s is the resulting dimension specified by the designer[p]. The performance output is defined by

$$\mathbf{z}(t) = \mathbf{H}\mathbf{x}(t), \tag{2.40}$$

where $\mathbf{H} \in \mathbb{R}^{N_s \times N_x}$ is a diagonal weighting matrix which can be chosen to be equal to the output matrix of the system ($\mathbf{C}$) to induce tracking on the output. $\mathbf{P} \geq \mathbf{0} \in \mathbb{R}^{N_s \times N_s}$ is the final tracking error weight. Similarly, $\mathbf{Q} \geq \mathbf{0} \in \mathbb{R}^{N_s \times N_s}$ is the tracking error weighting and $\mathbf{R} > \mathbf{0} \in \mathbb{R}^{N_u \times N_u}$ is the control weighting.

The optimal LQT can then be calculated from the solution of ($\mathbf{S} \in \mathbb{R}^{N_x \times N_x}$) in the following Riccati equation:

$$-\dot{\mathbf{S}}(t) = \mathbf{A}^\top\mathbf{S}(t) + \mathbf{S}(t)\mathbf{A} - \mathbf{S}(t)\mathbf{B}\mathbf{R}^{-1}\mathbf{B}^\top\mathbf{S}(t) + \mathbf{H}^\top\mathbf{Q}\mathbf{H} \quad \forall \quad t \leq T, \tag{2.41}$$

[p]Usually $N_s = N_y$

and $\mathbf{S}(T) = \mathbf{H}^\top \mathbf{P}\mathbf{H}$. The solution of $\mathbf{S}(t)$ in Eq. 2.41 is then used to give the optimal feedback gain:

$$\mathbf{K}(t) = \mathbf{R}^{-1}\mathbf{B}^\top \mathbf{S}(t), \tag{2.42}$$

where $\mathbf{K}(t) \in \mathbb{R}^{N_u \times N_x}$. The optimal feedback gain is used together with a feed-forward control to give the input

$$\mathbf{u}(t) = -\mathbf{K}(t)\mathbf{x}(t) + \mathbf{v}(t), \tag{2.43}$$

where $\mathbf{v}(t) \in \mathbb{R}^{N_u \times 1}$ is the feed-forward control defined by

$$\mathbf{v}(t) = \mathbf{R}^{-1}\mathbf{B}^\top \mathbf{w}(t), \tag{2.44}$$

where $\mathbf{w}(t) \in \mathbb{R}^{N_x \times 1}$ is input dependent and solved backward in time by the following differential equation:

$$-\dot{\mathbf{w}}(t) = (\mathbf{A} - \mathbf{B}\mathbf{K})^\top \mathbf{w}(t) + \mathbf{H}^\top \mathbf{Q}\mathbf{r}(t) \quad \forall \quad t \leq T, \tag{2.45}$$

and $\mathbf{w}(T) = \mathbf{H}^\top \mathbf{P}\mathbf{r}(T)$. Eqs. 2.44 & 2.45 can be merged to give the feed-forward control transfer function between $\mathbf{R}(s)$ and $\mathbf{V}(s)$ as

$$\mathbf{V}(s) = \mathbf{F}(s)\mathbf{R}(s) = \mathbf{R}^{-1}\mathbf{B}^\top \left[-s\mathbf{I} - (\mathbf{A} - \mathbf{B}\mathbf{K})^\top\right]^{-1} \mathbf{H}^\top \mathbf{Q}\mathbf{R}(s). \tag{2.46}$$

The LQT implementation is depicted in Fig. 2.20.

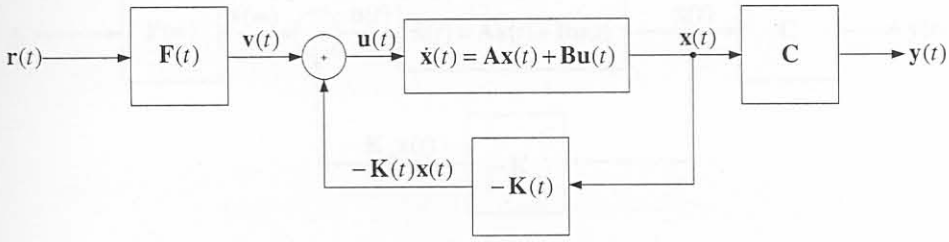

Figure 2.20 Linear quadratic tracker. Note that $\mathbf{F}(t) = \mathcal{L}^{-1}\{\mathbf{F}(s)\}$

2.2.5.3 Steady-state application

For some applications, certain conditions arise which makes the above solution to the LQT simpler. These conditions are:

1. The tracker must follow a constant input: $\mathbf{r}(t) = \mathbf{r}_0$.
2. The tracker is optimal at steady-state ($t \to \infty$).

Under the conditions above, Eq. 2.45 reduces to

$$\mathbf{w}(\infty) = \left[-(\mathbf{A} - \mathbf{B}\mathbf{K}_\infty)^\top\right]^{-1} \mathbf{H}^\top \mathbf{Q}\mathbf{r}_0, \tag{2.47}$$

where $\mathbf{w}(\infty)$ is constant and $\mathbf{K}_\infty$ is the optimal infinite horizon gain given by

$$\mathbf{K}_\infty = \mathbf{R}^{-1}\mathbf{B}^\top \mathbf{S}_\infty, \tag{2.48}$$

which optimises the infinite horizon performance index

$$J(t_0) = \frac{1}{2}\int_0^\infty \mathbf{e}^\top(t)\mathbf{Q}\mathbf{e}(t) + \mathbf{u}(t)\mathbf{R}\mathbf{u}^\top(t)dt, \tag{2.49}$$

$\mathbf{S}_\infty$ is the limiting solution to the time-varying Riccati equation and can be found by solving the algebraic Riccati equation (ARE)

$$0 = \mathbf{A}^\top \mathbf{S}_\infty + \mathbf{S}_\infty \mathbf{A} - \mathbf{S}_\infty \mathbf{B}\mathbf{R}^{-1}\mathbf{B}^\top \mathbf{S}_\infty + \mathbf{H}^\top \mathbf{Q}\mathbf{H}. \tag{2.50}$$

As a consequence of the above, Eq. 2.46 reduces to a time equivalent[q] of

$$\mathbf{v}(\infty) = \mathbf{R}^{-1}\mathbf{B}^\top \left[-(\mathbf{A} - \mathbf{B}\mathbf{K}_\infty)^\top\right]^{-1} \mathbf{H}^\top \mathbf{Q}\mathbf{r}_0 = \mathbf{F}(\infty)\mathbf{r}_0, \tag{2.51}$$

where $\mathbf{v}(\infty)$ is then a constant. Finally, the control law is implemented by

$$\mathbf{u}(t) = -\mathbf{K}_\infty \mathbf{x}(t) + \mathbf{v}(\infty), \tag{2.52}$$

The steady-state LQT (LQTSS) implementation is depicted in Fig. 2.21.

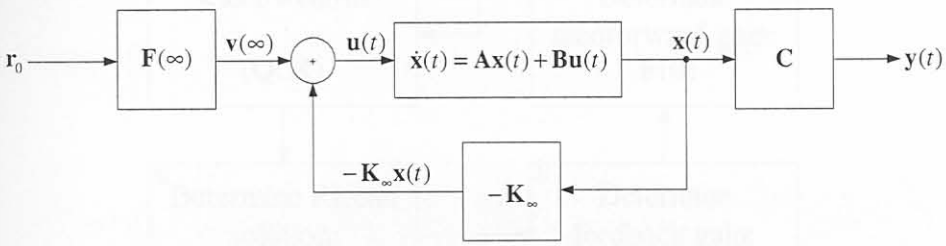

Figure 2.21 Linear quadratic tracker at steady-state.

2.2.5.4 Transfer function of the LQTSS

Using the result in §2.2.5.3 and replacing Eq. 2.51 in Eq. 2.52 and this result in Eq. 2.36 and Eq. 2.37 and simplifying, the following closed-loop state-space system results.

$$\dot{\mathbf{x}}(t) = (\mathbf{A} - \mathbf{B}\mathbf{K}_\infty)\mathbf{x}(t) + \mathbf{B}\mathbf{F}(\infty)\mathbf{r}(t), \quad \mathbf{x}(t_0) = \mathbf{x}_0 \tag{2.53}$$

$$\mathbf{y}(t) = (\mathbf{C} - \mathbf{D}\mathbf{K}_\infty)\mathbf{x}(t) + \mathbf{D}\mathbf{F}(\infty)\mathbf{r}(t), \tag{2.54}$$

[q]note that in the time domain, $\mathbf{F}(t)$ when t tends to infinity is denoted by $\mathbf{F}(\infty)$ and this same *constant* is denoted by $\mathbf{F}(0)$ in the s-plane, *i.e.* $\mathbf{F}(s \to 0) = \mathbf{F}(t \to \infty)$.

where $\mathbf{r}(t)$ is the desired trajectory of the output $\mathbf{y}(t)$. Assuming that the initial conditions are zero, the transfer function of the system above is given by

$$\mathbf{Y}(s) = \left\{[\mathbf{C} - \mathbf{D}\mathbf{K}_\infty][s\mathbf{I} - (\mathbf{A} - \mathbf{B}\mathbf{K}_\infty)]^{-1}\mathbf{B}\mathbf{F}(0) + \mathbf{D}\mathbf{F}(0)\right\}\mathbf{R}(s). \tag{2.55}$$

2.2.5.5 Design procedure

The design procedure for the steady-state LQT is shown in Fig. 2.22. The first step in the

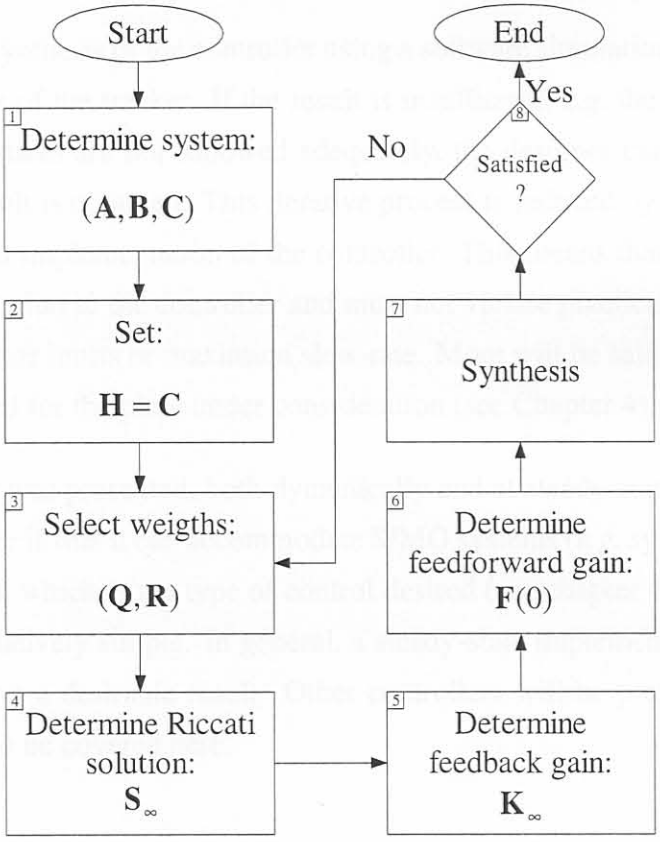

Figure 2.22 Design procedure for the LQTSS.

design procedure is to find an adequate state-space representation of the plant for which the LQTSS has to be designed. This step (step 1 in the figure) is critical to find an LQTSS that will minimise the performance index of Eq. 2.49.

Once the plant is known, step two is performed so that the tracker follows the outputs and not the state. This step is carried out by setting the weighting matrix $\mathbf{H}$ equal to the output matrix $\mathbf{C}$. For a linear first order system without any coupling between outputs, the mentioned procedure will be valid since the output and the state can be equal. Therefore only the

outputs need to be measured (same as measuring the states) and step 2 is then essentially left out of the implementation.

Step 3 requires the selection of the input and tracking error weighting matrices, $\mathbf{R}$ and $\mathbf{Q}$, respectively (see chapter 4 which discusses the selection procedure used in this work). Once the system is known and the weighting matrices have been selected, the next step is to determine the solution to the ARE. The result of step 4 is a solution of $\mathbf{S}_\infty$. With the solution of the ARE known, the feedback gain, $\mathbf{K}_\infty$ can be computed (step 5) and then the feed-forward gain $\mathbf{F}(0)$ may be computed next (step 6).

Step 7 involves the synthesis of the controller using a software simulation and then determining the effectiveness of the tracker. If the result is insufficient, *e.g.* the actuator constraints are violated or the states are not followed adequately, the designer can repeat steps 3 to 7 until the desired result is obtained. This iterative process is induced by step 8 and is necessary for the practical implementation of the controller. This means that the algorithm must find an adequate solution to the controller and must not violate practical constraints such as *e.g.* maximum actuator limits or maximum slew-rate. More will be said about this when the controller is designed for the plant under consideration (see Chapter 4).

The LQT controller was presented, both dynamically and at steady-state. The advantage of this type of controller is that it can accommodate SIMO systems (*e.g.* systems with one input and several outputs), which is the type of control desired (see chapter 4). The design of the controller is also relatively simple. In general, a steady-state implementation of the LQT is adequate [148] to get a desirable result. Other controllers will be presented later, and are simple enough not to be covered here.

2.3 Conclusion

A brief overview of the continuous casting process was given. A literature overview regarding the defects that are present during continuous casting was presented. Statistical hypothesis tests to determine whether an empirical distribution is part of some theoretical distribution were also presented. Correlation methods to determine linear dependence were given. Auto regression with exogenous input as a system identification procedure was perused and a special type of controller known as the linear quadratic tracker at steady-state was explained.